Open Ceramics 9 (2022) 100229

Contents lists available at ScienceDirect

Open Ceramics

journal homepage: www.sciencedirect.com/journal/open-ceramics

Kinetics of viscous flow sintering of glass–zircon composites. Effect of zircon volume fraction and particle size distribution

J.L. Amorós [a,b], E. Blasco [a,*], A. Moreno [a,b], C. Feliu [a,b]

[a] Instituto de Tecnología Cerámica, Asociación de Investigación de las Industrias Cerámicas, Spain
[b] Department of Chemical Engineering, Universitat Jaume I, Campus Universitario Riu Sec, 12006, Castellon, Spain

ARTICLE INFO

Keywords:
Sintering kinetics
Glass-ceramic composites
Percolation

ABSTRACT

Viscous flow sintering of glass–zircon composites was studied by isothermal and constant-rate heating experiments. The sintering curves fitted very well to the developed kinetic model, based on the Kohlrausch–Williams–Watts (KWW) function. Increasing the zircon volume fraction and decreasing the zircon–glass particle size ratio was verified to slow down the sintering rate. The combined effect of these variables on sintering was interpreted on the basis of percolation theory. The influence of temperature on the composite sintering rate corresponded to the influence of this variable on glass matrix flowability. Dimensionless relationships between the kinetic parameters and zircon volume fraction and the particle size ratio were obtained, which were independent of the thermal treatment used.

1. Introduction

Many fired bodies are composites of glass sintering particles (matrix) and non-sintering crystalline phase (inclusions), known as glass matrix composites (GMCs). Examples include glazes, low temperature co-fired ceramics, and substrates for electronic circuits. Viscous flow is the main sintering mechanism in these materials. However, even in the simplest GMCs, namely those in which the dissolution of inclusions in the glass is negligible and no phase separation or devitrification occurs in the glass, at high volume fractions of inclusions, ϕ, and/or the particle size distributions of inclusions and glass differ, sintering cannot be well described by the available kinetic models. The geometric arrangement of the rigid inclusions among the glass particles critically affects the effective viscosity and sintering rate of a composite. In a previous study, it was broadly concluded that sintering retardation was closely related to percolation of the inclusions [1–4]. It is generally understood that, when the inclusion volume fraction, ϕ, is sufficient, sintering stops completely [5]. This cessation of densification is often thought to coincide with the formation of inclusion percolation.

Previous studies examined the sintering of glass–zircon composites and the effect of the zircon volume fraction on the sintering curve under non-isothermal conditions and on the microstructure of the resulting materials [6,7]. In those studies, zircon particle size distribution (PSD) was much finer than that of glass PSD, so that the latest, most sophisticated models [8,9], which require both materials to exhibit the same particle size distribution, could not be applied. The sintering mechanism of these composites, for zircon volume fractions $\phi < 0.43$, was observed to be viscous flow; in contrast, for $\phi > 0.43$, composite densification also required the contribution of the zircon dissolution–reprecipitation mechanism. In addition, an increase in zircon content, ϕ, was verified to raise composite closed porosity, particularly for high ϕ contents. The variation of glass and zircon particle size distribution was also found to significantly affect composite sintering rate and microstructure [10].

1.1. Viscous flow sintering described by the KWW function. Interpretation of the relaxation time constant based on percolation theory

The Kohlrausch–Williams–Watts (KWW) function appropriately describes many irreversible dynamic processes of heterogeneous systems, for example the sintering of materials such as glasses [11], glazes [12–14], composites [6,7,10], and vitrified ceramic bodies [15]. This is probably due to the heterogeneity of these real systems on a microscopic scale, so that their overall behaviour, described by the KWW function, is the result of the weighted sum of a multitude of different simple processes, each of which is associated with a microvolume that has its own microstructural characteristics [16,17]. In the simplest interpretation, each of these different entities exhibits its own dynamic behaviour,

* Corresponding author.
E-mail address: encarna.blasco@itc.uji.es (E. Blasco).

https://doi.org/10.1016/j.oceram.2022.100229
Received 27 October 2021; Received in revised form 27 January 2022; Accepted 1 February 2022
Available online 2 February 2022

depending on its local microstructure, with its own time constant, τ_i, which differs from that of another region. This scenario led, in a previous paper [11], to a glass particle compact being deemed to comprise an almost infinite set of entities, with a corresponding relaxation spectrum or distribution of viscous sintering time constants, $\rho(\tau_i)$, that determine the value of the stretching parameter, n, and relaxation time, τ, of the KWW function (Eq. (1)), which describe compact densification kinetics.

$$\alpha = \frac{\varepsilon_V}{\varepsilon_{V,max}} = 1 - exp\left(-\frac{t}{\tau}\right)^n \quad \text{Eq. 1}$$

in which α is the degree of sintering progress, and ε_V and $\varepsilon_{V,max}$ are the instantaneous and maximum volume strain, respectively.

Therefore, in principle, Eq. (1), which describes glass particle viscous flow sintering very well [11], may also be assumed to appropriately describe composite densification, when other processes such as dissolution–reprecipitation of the inclusions do not occur. However, for the model (Eq. (1)) to be useful, it is essential to have a univocal relationship between each of these kinetic parameters, τ and n, and the volume fraction of inclusions, ϕ, and the ratio, ℜ, between the mean radius of the inclusion particles, r_i, and that of the matrix particles, r. In addition, it is advisable for these two kinetic parameters and their respective relationships with the characteristics of the composite to have a clear physical meaning, so that the results obtained can be applied to other systems. To achieve this objective, the following assumptions were made:

(i) Relaxation sintering time, τ (Eq. (1)), for a composite is assumed to be analogous to that of a glass compact, $\tau(\phi = 0)$, however, replacing glass viscosity, η, with composite effective viscosity, η_{eff}. Therefore, for a glass particle compact [11], one obtains:

$$\tau(\phi = 0) = \Omega\tau_g = \Omega\frac{\eta r}{\gamma} \quad \text{Eq. 2}$$

in which Ω is a numerical constant, τ_g is viscous sintering time, and η, γ, and r are glass viscosity, surface tension, and particle mean radius, respectively. And for a composite one obtains:

$$\tau = \Omega\frac{\eta_{eff} r}{\gamma} \quad \text{Eq. 3}$$

This approach is equivalent to assuming that the ratio between composite sintering rate and glass matrix sintering rate is equal to the ratio between glass viscosity and composite viscosity [5,18], as has been verified for composites of identical spherical particles ($r_i = r$).

(ii) The effective viscosity of a composite of same-sized spherical particles, with a volume fraction of inclusions, ϕ, was related to glass viscosity,η, by the equation [5,18]:

$$\frac{\eta_{eff}}{\eta} = \left(1 - \frac{\phi}{\phi_p}\right)^{-m} \quad \text{Eq. 4}$$

in which $m > 0$ and ϕ_p is the rigid percolation threshold [19], that is, the volume fraction of inclusions at which these inclusions percolate and cause the material's behaviour to be rigid. The value of ϕ_p is always greater than the value of the conductive percolation threshold, ϕ_p^c. Indeed, ϕ_p^c, is the minimum volume fraction of inclusions for a cluster of inclusions to form that extends throughout the entire thickness of the packing connecting the two faces of a plate. This is always smaller than ϕ_p, which is the minimum volume fraction for generating a cluster of inclusions that extends throughout the entire thickness of the packing and is able to support the load without deforming. The value of ϕ_p, for packings of same-sized spheres, depends on the nature of the inclusion–inclusion interaction [5]. For sliding contacts $\phi_p = 0.96$, for frictional contacts $\phi_p = 0.57$ and, only for strongly bonded contacts, $\phi_p = \phi_p^c = 0.33$.

(iii) For values of $\Re \neq 1$, Eq. (4) is still assumed to be valid, but with a value of ϕ_p that depends on ℜ. Unfortunately, values of ϕ_p are unavailable for $\Re \neq 1$. Values of ϕ_p^c are only estimated as a function of ℜ. The values of ϕ_p^c are plotted versus the size ratio, ℜ, obtained by different researchers, in Fig. 1. For sizes of inclusions, r_i, much larger than those of matrix particle size, r, that is, $\Re >>> 1$, the values of the conductive percolation threshold, ϕ_p^c, predicted by different models are high (up to 0.8–0.9); in addition, in this case, the matrix particles need to position themselves in the voids formed by the dense packing of rigid inclusions, in accordance with the theoretical models [20,21] and numerical simulations [21]. Under these conditions, it may be assumed that the inclusion aggregates that form are rigid, i.e. are able to support the entire load, so that $\phi_p^c = \phi_p$. For $\Re <<< 1$, the opposite occurs, i.e. the small rigid inclusions are located in the voids left by the soft particle packing of the matrix, so that $\phi_p^c <<< \phi_p$. Therefore, the difference between ϕ_p and ϕ_p^c may be assumed to increase as ℜ decreases. In accordance with this assumption and with the value of $\phi_p = 0.57$ calculated for $\Re = 1$ [5], the assumed values of ϕ_p have been plotted by means of a blue area in Fig. 1. Thus, as ℜ increases, ϕ_p also rises, so that, keeping the other variables, ϕ and temperature, constant, composite effective viscosity, η_{eff}, decreases. Eq. (4) thus describes the joint effect of ϕ and ℜ on the effective viscosity of the system.

(iv) The effect of temperature on effective viscosity, η_{eff}, is assumed to be that of this variable on glass viscosity, η, that is, the effect described by the Vogel–Fulcher–Tammann (VFT) equation:

$$\eta = \eta_0 exp\left(\frac{B}{T - T_{VFT}}\right) \quad \text{Eq. 5}$$

in which η_0, B, and T_{VFT} are the equation parameters.

(v) From Eq. (3) and Eq. (4) one obtains:

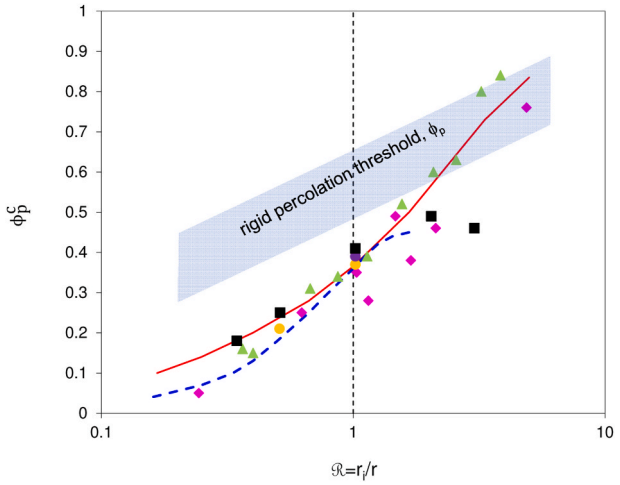

Fig. 1. Conductive percolation threshold, ϕ_p^c, versus the ratio $\Re = r_i/r$. Dashed blue line: results of Kuo and Gupta [23] using the Bouvard and Lange model [20]. Solid red line: results of Kuo and Gupta [23] using the Suzuki and Oshima model [24]. Green triangles: results of the Oger et al. numerical simulation [25]. Pink rhombuses: experimental results obtained by Oger et al. [25]. Black squares: results of the Bouvard and Lange numerical simulation [20]. Yellow circles: extrapolated results of the experimental values obtained by Fitzpatrick et al. [26]. Purple circle: results of the Powell numerical simulation [27]. Blue area: values of the rigid percolation threshold, ϕ_p, assumed by the authors. (For interpretation of the references to colour in this figure legend, the reader is referred to the Web version of this article.)

$$\tau = \Omega \frac{\left(1-\frac{\phi}{\phi_p}\right)^{-m} r\eta}{\gamma} \quad \text{Eq. 6}$$

And from Eq. (2) and Eq. (6):

$$\tau = \Omega\left(1-\frac{\phi}{\phi_p}\right)^{-m}\tau_g = \left(1-\frac{\phi}{\phi_p}\right)^{-m}\tau(\phi=0) \quad \text{Eq. 7}$$

Thus, composite relaxation time, τ, which is always greater than that of the matrix, τ(ϕ=0), increases with the volume fraction of inclusions, ϕ, and decreases with size ratio, ℜ, (since ϕ_p increases as ℜ does).

(vi) In the ideal case of sphere packings, the size and number of inclusion clusters that form have been verified to increase with the volume fraction of inclusions, ϕ, and with the decrease in ℜ, [20,22–27]. This leads to a heterogeneous microstructure made up of an array of regions or entities with different characteristics. However, composites are prepared from different particle size distributions of inclusions and glass, and the resulting formed unfired particle packing is not ideal, causing the heterogeneity of the particle size distributions of the inclusions and matrix to be even greater than that predicted by the models. These microstructural heterogeneities lead the composite to be made up of an array of different regions or entities, with a corresponding relaxation time distribution that widens as ϕ increases and ℜ decreases. As a result, kinetic parameter n, related to the amplitude of the relaxation time distribution [16,17,28], decreases as ϕ increases and ℜ decreases.

1.2. Kinetic equations

Rearranging Eq. (1) yields the expression:

$$\frac{t}{\tau} = g(\alpha) = [-ln(1-\alpha)]^{\frac{1}{n}} \quad \text{Eq. 8}$$

in which g(α) is the integrated form of the kinetic model.

Analogously, the sintering rate (differential form of the kinetic model) is given by:

$$\frac{d\alpha}{dt} = \frac{1}{\tau}f(\alpha) = \frac{1}{\tau}n(1-\alpha)[-ln(1-\alpha)]^{\frac{n-1}{n}} \quad \text{Eq. 9}$$

In isothermal treatments [11], when the kiln reaches the programmed temperature (isothermal treatment start t = 0), the test piece has already undergone a certain shrinkage and, hence, a degree of initial progress (α = α_0). To process the results, it is therefore necessary to integrate Eq. (9), taking as initial condition: t = 0 → α = α_0, which yields:

$$\alpha = 1 - \frac{1}{exp\left\{\frac{t}{\tau} + [-ln(1-\alpha_0)]^{1/n}\right\}^n} \quad \text{Eq. 10}$$

Assuming the effect of temperature on process relaxation time to be the same as the effect of this variable on glass viscosity [6,7,11], from Eq. (5) and Eq. (6) one obtains:

$$\tau = \tau_0 exp\left(\frac{B}{T-T_{VFT}}\right) \quad \text{Eq. 11}$$

in which τ_0 is given by:

$$\tau_0 = \Omega\left(1-\frac{\phi}{\phi_p}\right)^{-m}\frac{\eta_0 r}{\gamma} = \Omega\tau_{g0}\left(1-\frac{\phi}{\phi_p}\right)^{-m} = \tau_0(\phi=0)\left(1-\frac{\phi}{\phi_p}\right)^{-m} \quad \text{Eq. 12}$$

For a process at constant-rate heating, β, from Eq. (9) and Eq. (11) one obtains:

$$\frac{d\alpha}{dT} = \frac{1}{\tau_0\beta}exp\left(-\frac{B}{T-T_{VFT}}\right)f(\alpha) \quad \text{Eq. 13}$$

Separating variables and integrating yields the integral form of the sintering model, g(α), and its relationship to temperature. Using the Murray and White approximation [29], one obtains:

$$g(\alpha) = \int_0^\alpha \frac{d\alpha}{f(\alpha)} = \frac{1}{\tau_0\beta}\int_0^T exp\left(-\frac{B}{T-T_{VFT}}\right)dT = \frac{(T-T_{VFT})^2}{\tau_0\beta B}exp\left(-\frac{B}{T-T_{VFT}}\right) \quad \text{Eq. 14}$$

Replacing g(α) with Eq. (8) in Eq. (14) and operating yields:

$$\alpha = \frac{\varepsilon_V}{\varepsilon_{V,\,max}} = 1 - exp\left\{-\left[\frac{(1+\kappa\beta)}{\tau_0\beta}\frac{(T-T_{VFT})^2}{B}exp\left(-\frac{B}{(T-T_{VFT})}\right)\right]^n\right\} \quad \text{Eq. 15}$$

in which κ is an empirical constant. In this equation, the factor $(1+\kappa\beta)$ [11,14] is introduced to take into account the real heating rate of the test piece being lower than the programmed rate, β, as, to all effects, raising the heating rate increases the temperature difference between the kiln and the piece.

The objectives of this study were as follows: to verify the validity of the model developed for glasses [11], based on the KWW function, for describing composite viscous flow sintering; to interpret the physical meaning of the stretching parameter, n, and relaxation time, τ, of the kinetic equation; and to relate these kinetic parameters to the volume fraction of inclusions, ϕ, and to the ratio between inclusion mean particle size and matrix mean particle size, ℜ = r_i/r, based on percolation theory. These last two characteristics of the filler largely determine the firing behaviour and properties of composites, both used as coatings [30,31] and pieces [32–34]. To validate the kinetic model, isothermal and constant-heating rate experiments were carried out, since, for a kinetic model to be applicable, the values of the kinetic parameters obtained by both methods must be the same.

2. Materials and experimental procedure

A borosilicate frit of composition close to that of glass SRM 717a [35] used in previous papers [6,7,11] was selected. Its viscosity curve fitted very well to the Vogel–Fulcher–Tammann (VFT) equation [6,11,35]:

$$log\eta = -3.012 + \frac{5495.3}{T-148.1} \quad \text{Eq. 16}$$

in which viscosity, η, is expressed in Pa·s and T is temperature in °C. Glass surface tension, estimated from the glass composition by the Dietzel equation [11,36], was γ = 0.277 N/m. The frit particles were wet milled for 30min in an alumina ball mill until particle size distribution (PSD) G_M was obtained. Frit particle suspension G_M was milled anew in a zirconia bead mill to obtain a finer PSD, G_F. Two industrial zircon powders (micrometric and flour), and a mixture of these, were selected as rigid inclusions. The PSD of frit G_M and G_F, and of micrometric and flour zircon, Z_M and Z_F, was determined with a laser diffraction instrument (Fig. 2). The G_M, G_F, and Z_M PSDs fitted very well to lognormal distributions; in contrast, the Z_F PSD fitted very well to the Weibull model (Table 1 and Fig. 2).

To determine the effect of the zircon and glass particle size distributions on sintering, glass–zircon mixtures were prepared, at a constant zircon volume fraction, ϕ = 0.32. The batch formulas, nomenclature, and ratio of inclusion particle radius/glass particle radius, ℜ = r_i/r, are detailed in Table 2. To study the effect of the zircon volume fraction, ϕ, G_MZ_M mixtures with values of 0.05 ≤ ϕ ≤ 0.43 were prepared. It was confirmed elsewhere [6,7,10] that, for these mixtures, sintering took place exclusively by viscous flow. For values of ϕ ≥ 0.53, complete

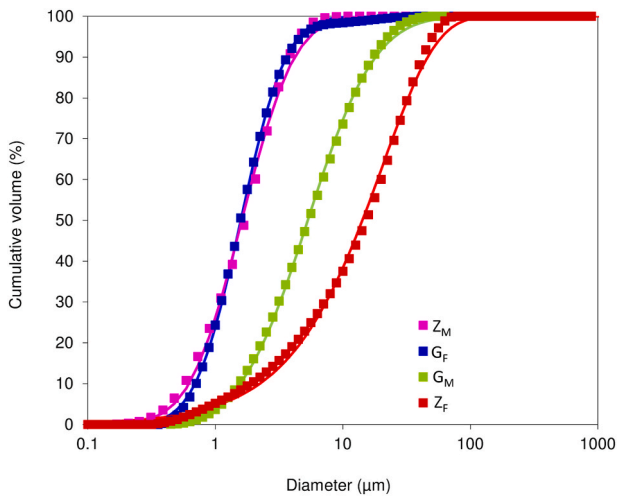

Fig. 2. Particle size distribution (PSD) of the G_M, G_F, Z_M, and Z_F materials determined by laser diffraction. The G_M, G_F and Z_M PSDs were fitted to the lognormal distribution and the Z_F PSD to the Weibull distribution.

densification of the composite required contribution of the zircon solution–reprecipitation mechanism [6,7,10]. The mixtures were prepared by wet milling in an alumina ball mill. To avoid segregation of the components, the suspensions were subjected to colloidal filtration and subsequent oven drying.

Cylindrical test pieces, about 5 × 3mm, were pressed at 30 MPa, following the procedure described in a previous paper [11]. The sintering curves were determined from the initial, A_0, instantaneous, A, and minimum, A_{min}, silhouette surface areas of the test pieces by heating microscopy (HSM), at constant-rate-heating ($2 \leq \beta \leq 60$K/min) and isothermal heat treatments. Diametral and axial strains were similar until completion of sintering. Once the sintering process had been completed, test piece geometry changed [13]. Assuming isotropic shrinkage, the sintering progress parameter, α, was calculated as:

$$\alpha = \frac{\varepsilon_V}{\varepsilon_{V,\,max}} = \frac{\varepsilon_A}{\varepsilon_{A,\,max}} = \frac{ln(A/A_0)}{ln(A_{min}/A_0)} \qquad \text{Eq. 17}$$

3. Results and discussion

3.1. Influence of the zircon volume fraction, φ. composites G_MZ_M

To study the effect of the zircon volume fraction, ϕ, on composite sintering, five mixtures were prepared (ϕ = 0.05, 0.105, 0.17, 0.32, and 0.43) from glass with particle size distribution G_M and from micronised zircon, Z_M.

3.1.1. Isothermal sintering

For each of these composites, a series of isothermal experiments were carried out at different temperatures. The sintering curves of some composites: ϕ = 0.105, ϕ = 0.32, and ϕ = 0.43 are plotted in Fig. 3. The pairs of values (α, t) were fitted to Eq. (10). For each composite, the values of n varied very little and did so randomly. A second fit was therefore performed, keeping a constant value of n for each composite. The fit of the experimental data and the calculated values was very good in every case (Fig. 3). Kinetic parameter n decreased linearly with zircon volume fraction (Fig. 4), as had been assumed (point (vi) of Section 1.1).

On plotting, for each composite, on a logarithmic scale (Fig. 5), the values of relaxation time τ, obtained on fitting the corresponding isothermal curves to Eq. (10) versus the respective viscous sintering times, τ_g (Eq. (2)), calculated from the viscosity, η, value given by the VFT equation (Eq. (5)) and taking γ = 0.277 N/m, straight lines with unit slope and ordinate at the origin were obtained, the ordinate being higher as zircon content, ϕ, increased These results confirmed that the influence of temperature on relaxation time, τ, was due to the effect of this variable on glass flowability (or inverse of its viscosity) and that, with the increase in zircon content, ϕ, τ increased, this rise being greater as ϕ rose. These results are consistent with the developed model, which assumes that the increase in zircon content, ϕ, raises composite effective viscosity (Eq. (4)), and with it, the values of the relaxation time ratios τ/τ_g (Fig. 6) and $\tau/\tau(\phi = 0)$ (Fig. 7), in accordance with Eq. (7).

3.1.2. Non-isothermal sintering

The sintering curves obtained for each composite at heating rates of $2 \leq \beta \leq 60$ K/min were fitted to Eq. (15). Parameters κ, τ_0, and n were assumed as fitting parameters, which depended on zircon content, ϕ. The model was verified to appropriately describe the effect of the heating rate, β, on the sintering curves of all the studied composites. By way of example, the results corresponding to ϕ = 0.32 and the values of

Table 1
Particle size distribution (PSD) of each material. Fitting parameters of the lognormal (d_{NL} and σ) and Weibull (d_W and m) distributions and volume mean diameter, d_V.

Fit	PSD	Zircon Flour, Z_F	Micrometric Zircon, Z_M	Medium Glass, G_M	Fine Glass, G_F
Lognormal distribution	d_{NL} (μm)		1.62	5.32	1.58
	σ		2.11	2.60	1.90
Weibull	d_W (μm)	14.2			
	m	1.0			
	d_v (μm)	21.0±1.4	2.0±0.12	7.8±0.5	2.1±0.14

Table 2
Batch formulas (% by wt) and ratio of the zircon to glass particle volume mean radius (r_i/r) of composites with ϕ = 0.32.

Glass		Zircon			Composite	
G_M r = 3.9±0.25 μm	G_F r = 1.05±0.07 μm	Z_M r_i = 1.0±0.06 μm	Z_{MF} r_i = 4.9±0.3 μm	Z_F r_i = 10.5±0.7 μm	Reference	$\Re = r_i/r$
100					G_M	
	100				G_F	
50		50			G_MZ_M	0.26±0.03
50			50		G_MZ_{MF}	1.26±0.16
50				50	G_MZ_F	2.69±0.35
	50	50			G_FZ_M	0.95±0.12
	50		50		G_FZ_{MF}	4.67±0.60
	50			50	G_FZ_F	10.0±1.3

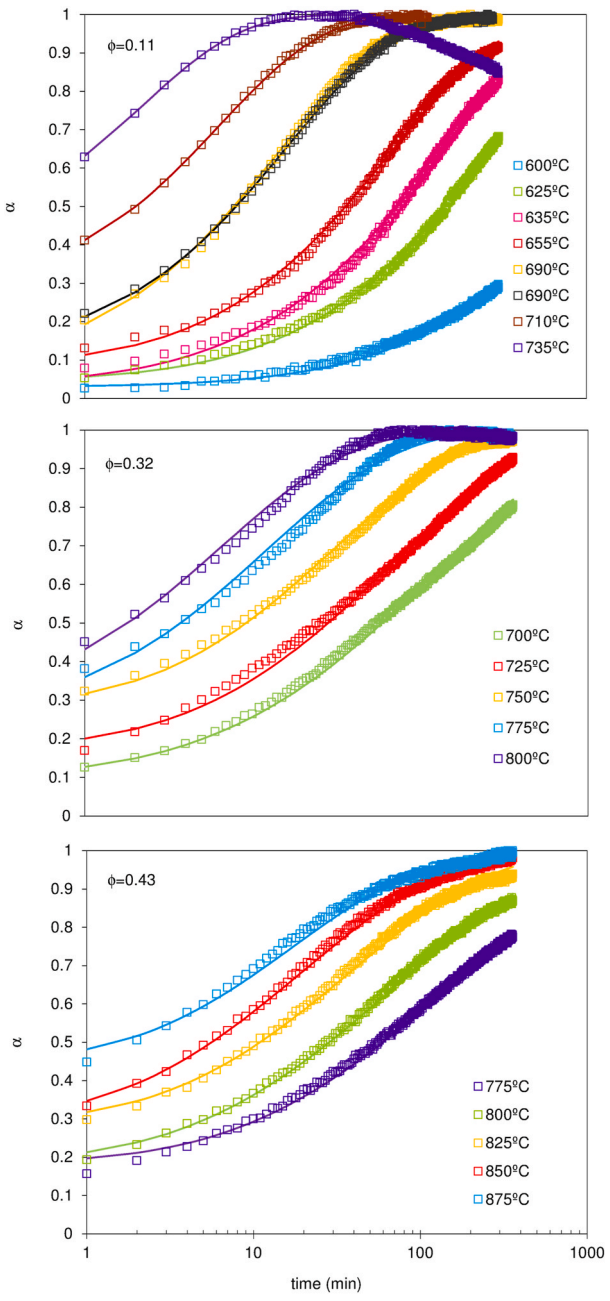

Fig. 3. Isothermal sintering curves. The symbols are experimental data, and the solid lines correspond to the values calculated from the model (Eq. (10)). Composites G_MZ_M with $\phi = 0.11$, 0.32, and 0.43.

the fitting parameters are indicated in Fig. 8.

The model was further verified to appropriately describe the effect of zircon content on the sintering curve, assuming a value of κ, τ_0, and n for each value of ϕ. The effect of ϕ on the sintering curve at a heating rate of $\beta = 15$K/min is shown in Fig. 9. In addition, the variation of n with zircon content, ϕ, was confirmed to be the same as that exhibited in isothermal sintering (Fig. 4). Analogously, the variations exhibited by the relaxation time ratios τ_0/τ_{0g} and $\tau_0/\tau_0(\phi = 0)$ with ϕ (Figs. 6 and 7, respectively) were predicted by Eq. (12), and they practically coincided with those exhibited by τ/τ_g and $\tau/\tau(\phi = 0)$, obtained from the isothermal experiments (Figs. 6 and 7).

In general, as zircon content, ϕ, increased, $-\varepsilon_A$ decreased (Fig. 10), as a rise in zircon content, ϕ, reduced unfired porosity while also raising attainable minimum porosity [6,7,10]. Both factors lowered maximum firing shrinkage.

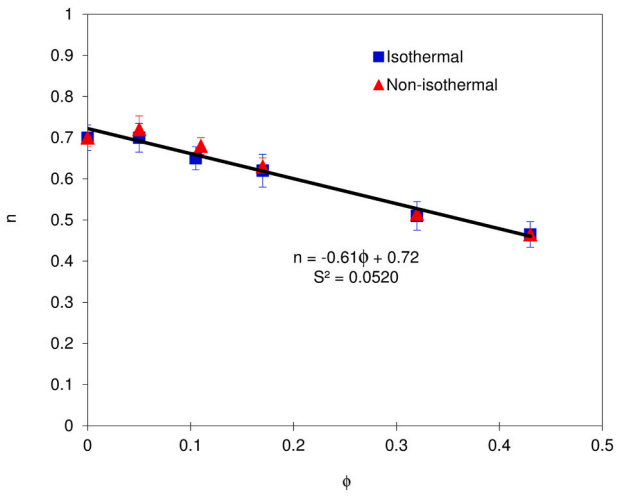

Fig. 4. Effect of zircon volume fraction, ϕ, on the stretching parameter, n. Isothermal (blue squares) and non-isothermal experiments (red triangles). Composites G_MZ_M. The solid line is the fit to the equation shown. (For interpretation of the references to colour in this figure legend, the reader is referred to the Web version of this article.)

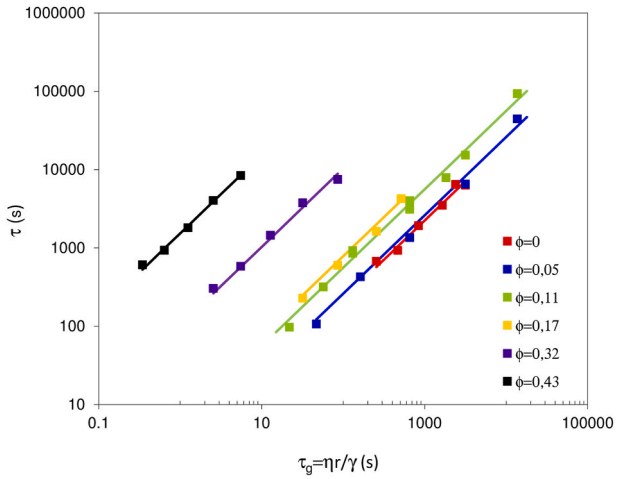

Fig. 5. Relationship between the values of experimental relaxation time, τ, and those of viscous sintering time, τ_g. Glass G_M ($\phi = 0$) and composites G_MZ_M with $\phi = 0.05$, 0.11, 0.17, 0.32, and 0.43.

It was verified (Fig. 11) that, at the same heating rate, β, as zircon content, ϕ, increased, the temperature at which the composite reached maximum shrinkage, T_f, and the range of sintering temperatures, difference between T_f and process onset temperature, T_i, rose considerably. In contrast, temperature T_i hardly changed. These results are consistent with assumption (vi) in Section 1.1, as the increase in sintering range stemmed from an increase in relaxation time distribution amplitude, which increased as n decreased. These results are also consistent with the results predicted by percolation theory [20,22]. Indeed, including for high inclusion contents ($\phi \approx 0.45$), glass particle volume fraction and connectivity were sufficiently high for microregions or entities made up exclusively of glass particles to form. As a result, the lower bound of the relaxation time distribution, $\rho(\tau_i)$, was associated with these microregions. In contrast, as the volume fraction of inclusions, ϕ, increased, much higher local inclusion volume fractions were reached in some microregions than the overall inclusion volume fraction, ϕ. The upper bound of the relaxation time distribution was therefore fixed by the regions with a larger amount of inclusions, with much longer relaxation times, which increased as ϕ rose. Thus, on plotting T_i, T_f, and T_f-T_i versus

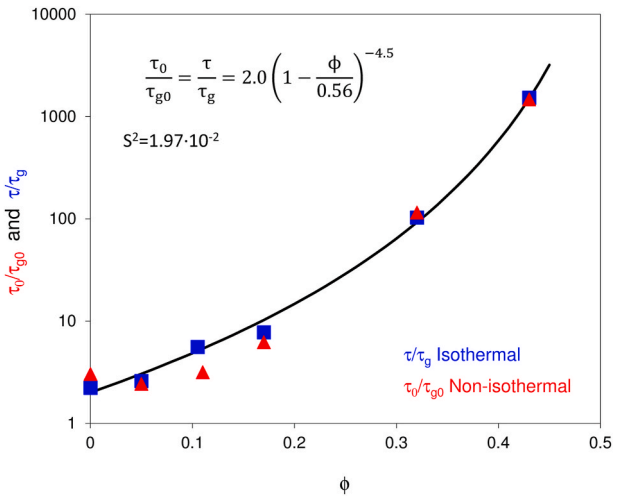

Fig. 6. Effect of zircon volume fraction, ϕ, on the values of the ratio τ/τ_g, obtained in isothermal experiments (blue squares), and the ratio τ_0/τ_{g0}, obtained in non-isothermal experiments (red triangles). Composites G_MZ_M. The solid line is the fit to the equation shown. (For interpretation of the references to colour in this figure legend, the reader is referred to the Web version of this article.)

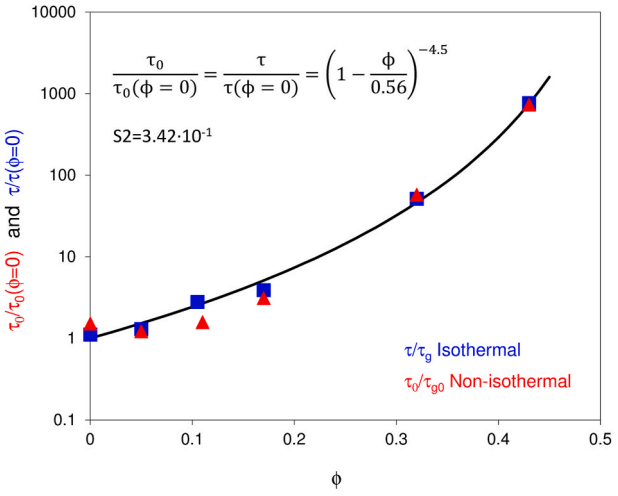

Fig. 7. Effect of zircon volume fraction, ϕ, on the values of the ratio $\tau/\tau(\phi = 0)$, obtained in isothermal experiments (blue squares), and the ratio $\tau_0/\tau_0(\phi = 0)$, obtained in non-isothermal experiments (red triangles). Composites G_MZ_M. The solid line is the fit to the equation shown. (For interpretation of the references to colour in this figure legend, the reader is referred to the Web version of this article.)

1/n (Fig. 12), they were observed to increase exponentially with ϕ. In the case of the sintering range, T_f-T_i, its correlation with 1/n, directly related to the relaxation time distribution amplitude, $\rho(\tau_i)$, was very good.

3.2. *Influence of the ratio of zircon particle mean radius to glass particle mean radius, $\Re = r_i/r$. Composites $\phi = 0.32$*

To study the effect of the ratio of zircon particle mean radius to glass particle mean radius, $\Re = r_i/r$, six composites with a zircon volume fraction $\phi = 0.32$ and different glass and zircon particle size distributions (Table 2) were prepared with a view to obtaining values of $\Re$ that ranged from $0.26 \leq \Re \leq 10$.

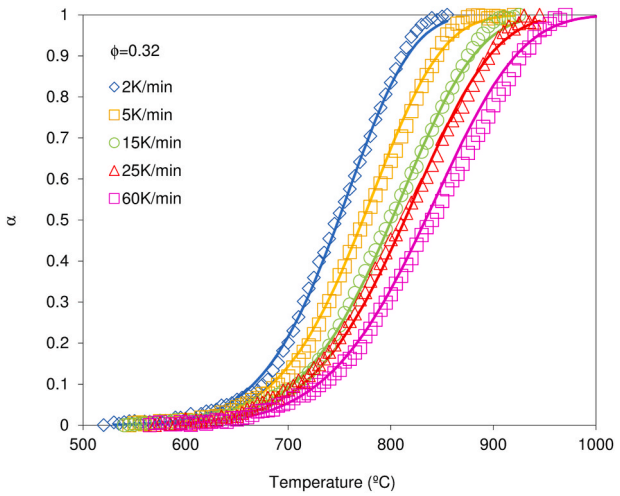

Fig. 8. Effect of heating rate on the non-isothermal sintering curves. The symbols are experimental data, and the solid lines correspond to the values calculated from the model (Eq. (15)), with τ_0=1.27·10^{-6} s, n=0.515, and κ=0.0121 min/K. Composite G_MZ_M with ϕ=0.32.

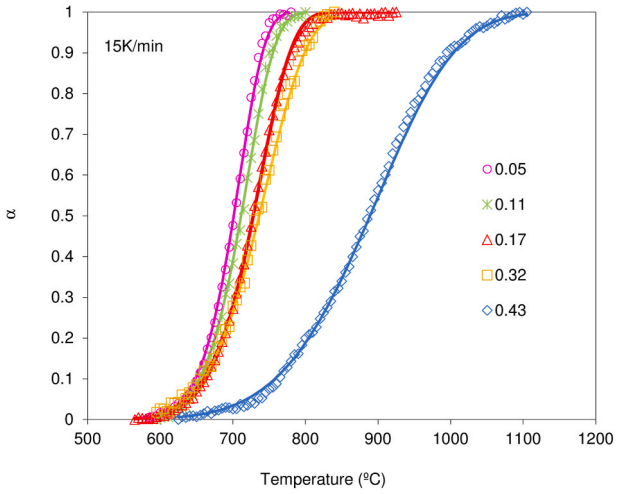

Fig. 9. Effect of zircon volume fraction, φ, on the non-isothermal sintering curves at β = 15K/min. The symbols are experimental data, and the solid lines correspond to the values calculated from the model (Eq. (15)). Composite G_MZ_M.

3.2.1. *Isothermal sintering*

Isothermal sintering curves were obtained for each of these composites and for each glass particle size distribution (Table 2) at different temperatures. The pairs of values (α, t), for each temperature and composition, were fitted to Eq. (10), keeping n constant for each composite. Good agreement was obtained in every case between the experimental data and the values calculated using the model. The effect of temperature on sintering of the composite prepared with the finest glass particle size distribution and the mixture of micronised zircon and zircon flour, G_FZ_{MF}, is shown in Fig. 13.

The sintering curves at 725 °C of the three composites prepared using glass particle size distribution G_M as matrix and zircon from the three studied zircon particle size distributions: Z_M, Z_F, and Z_{MF} (Table 2), as inclusions, are plotted in Fig. 14. The curves obtained at 675 °C for the composites prepared from the three zircon particle size distributions and glass G_F are plotted in Fig. 15. In every case, the fit of the experimental data to the values calculated using the model (Eq. (10)) was very good. In addition, in both cases, as the size of the inclusions increased, the sintering rate also rose. Indeed, at the same thermal treatment

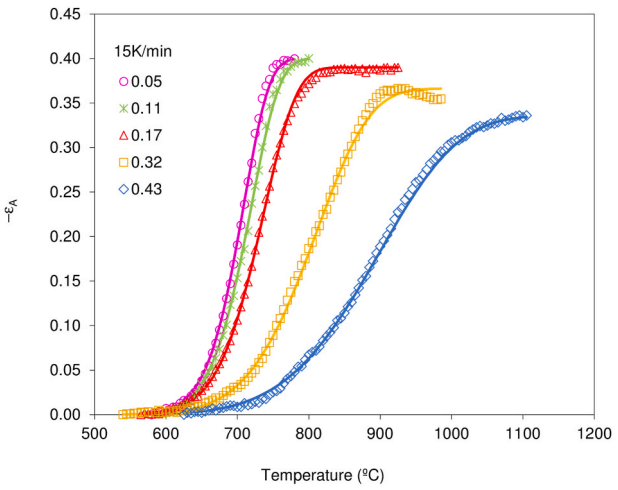

Fig. 10. Effect of zircon volume fraction, ϕ, on the curves: surface strain–temperature, ε_A-T, at β = 15K/min. The symbols are experimental data, and the solid lines correspond to the values calculated from the model (Eq. (15)). Composite G_MZ_M.

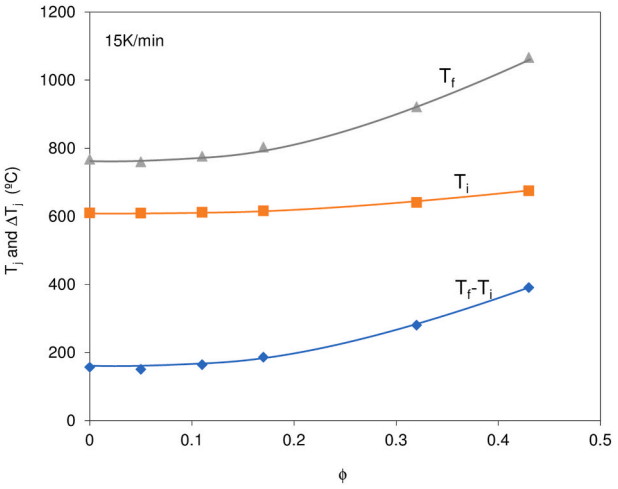

Fig. 11. Effect of zircon volume fraction on onset sintering temperature, T_i, final sintering temperature, T_f, and sintering temperature range, T_f-T_i. Composite G_MZ_M. Heating rate β = 15K/min.

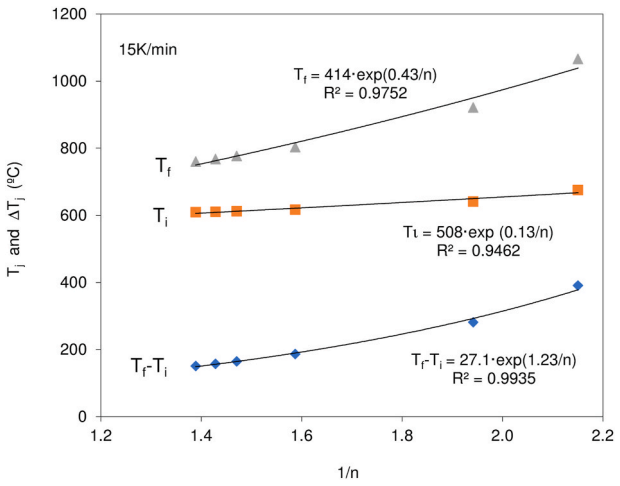

Fig. 12. Relationships between onset sintering temperature, T_i, final sintering temperature, T_f, and sintering temperature range, T_f-T_i, and the inverse of the stretching parameter, 1/n. The symbols are experimental data, and the solid lines are the fit to the equation shown. Composite G_MZ_M. Heating rate β = 15K/min.

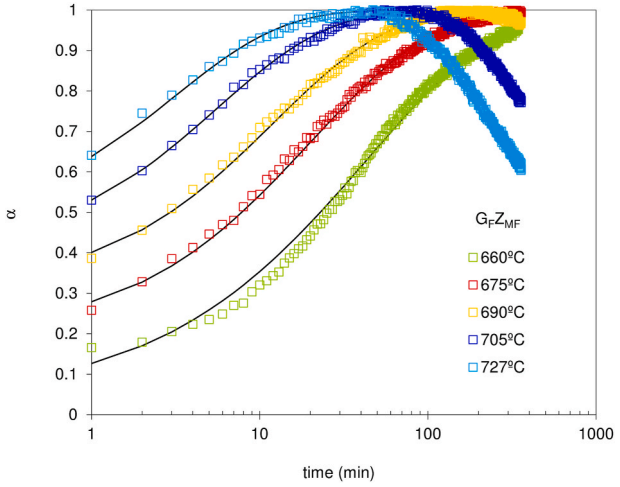

Fig. 13. Effect of temperature on the isothermal sintering curves. The symbols are experimental data, and the solid lines correspond to the values calculated from the model (Eq. (10)). Composites G_FZ_{MF} with ϕ = 0.32.

temperature and time, the highest degree of process progress, α, always corresponded to the composites prepared with the largest-sized zircon particles. This occurred because, at the same zircon content, ϕ, and glass particle size, r, as inclusion size, r_i, increased, the number of glass–glass contacts increased, the zircon–zircon contacts decreased, and the number and size of zircon clusters also decreased, which raised the sintering rate and reduced the effective viscosity of the composite. In addition, ϕ_p increased when ℜ rose, in accordance with Fig. 1, which translated into a decrease in effective viscosity of the composite, η_{eff}, (Eq. (4)) and in sintering relaxation time, τ, (Eq. (6) and Eq. (7)).

The effect of the size ratio, ℜ = r_i/r, on kinetic parameter n is shown in Fig. 16. A slight increase in n with ℜ may be observed, as had been assumed in point (vi) of Section 1.1, this relation being independent of glass matrix particle size distribution. However, the effect of ℜ on n was relatively small, as a variation of ℜ of two orders of magnitude only changed the value of n from 0.49 to 0.57.

As was done in Section 3.1.1, to verify the validity of Eq. (7), the values of relaxation time, τ, obtained on fitting the experimental data to Eq. (10), were plotted versus τ_g on a logarithmic scale in Fig. 17. The results fitted very well to straight lines of unit slope, whose ordinate at the origin decreased as the size ratio, ℜ = r_i/r, increased. Indeed, on plotting the quotient τ/τ_g versus ℜ (Fig. 18), a considerable decrease in τ/τ_g was observed with the rise in ℜ. This occurred because, as ℜ increased, the percolation volume fraction, ϕ_p, rose (Eq. (7)).

3.2.2. *Non isothermal sintering*

The sintering curves obtained at heating rates of 2≤β ≤ 60 K/min for each of the composites and glass compacts were fitted to Eq. (15). As in Section 3.1.2, the fitting parameters assumed for each material were κ, n, and τ_0, as they were independent of the heating rate, β. The model satisfactorily described the effect of heating rate, β, and size ratio, ℜ = r_i/r, on the sintering curves, as may be observed in Fig. 19 and Fig. 20. The experimental sintering curves, obtained at β = 15K/min, and the sintering curves calculated from the model (Eq. (15)), corresponding to composites prepared from the three zircon and glass G_M particle size distributions, and that of glass G_M, are plotted in Fig. 19. Similarly, the results of the series of composites prepared with the three zircon and glass G_F particle size distributions, and that of glass G_F, are plotted in Fig. 20. For the two glass particle size distributions used, the sintering

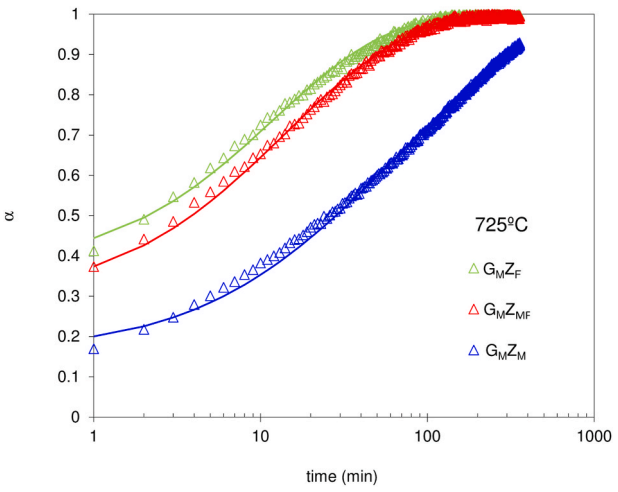

Fig. 14. Effect of zircon particle size, r_i, on the isothermal sintering curves. The symbols are experimental data, and the solid lines correspond to the values calculated from the model (Eq. (10)). Composites of glass G_M, with ϕ=0.32, fired at 725 °C.

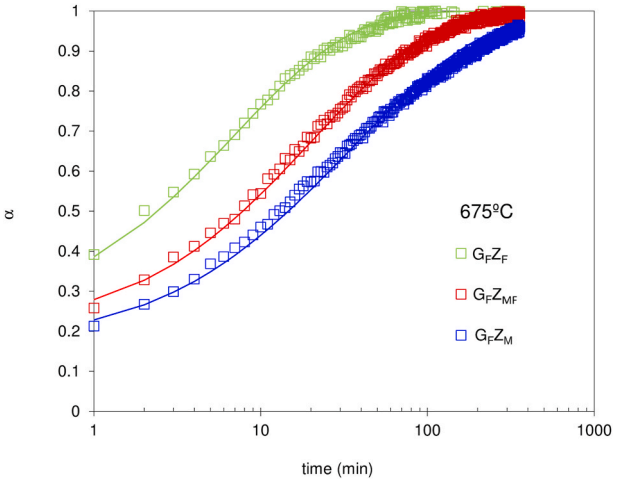

Fig. 15. Effect of zircon particle size, r_i, on the isothermal sintering curves. The symbols are experimental data, and the solid lines correspond to the values calculated from the model (Eq. (10)). Composites of glass G_F, with ϕ = 0.32, fired at 675 °C.

curves were observed to shift towards higher temperatures and their sintering range increased as zircon size decreased. This behaviour was accurately described by the increase in relaxation time, τ, and in kinetic parameter n with ℜ, as occurred in isothermal sintering and in accordance with point (iii) and (vi) of Section 1.1. The effect of size ratio, ℜ, on these parameters is shown in Figs. 16 and 18, together with the results obtained in isothermal treatment. The value of these parameters was verified to be practically independent of the thermal treatment used. For each parameter, the results fitted very well to the equations shown in Figs. 16 and 18. In every case, these equations predicted a slight increase in n and a considerable decrease in τ with ℜ. For values of ℜ→∞, both n and τ approached those of the glass, as the number of glass–glass contacts also did so.

In general, for all these composites it was verified that, as zircon size increased, linear shrinkage, $-\varepsilon_A$, decreased, owing to a reduction in composite initial porosity and to an increase in resulting minimum porosity [10]. The experimental data and the values calculated from Eq. (15), corresponding to the series of composites prepared with glass G_M particle size distribution, and that of glass G_M, at 15K/min, are shown in

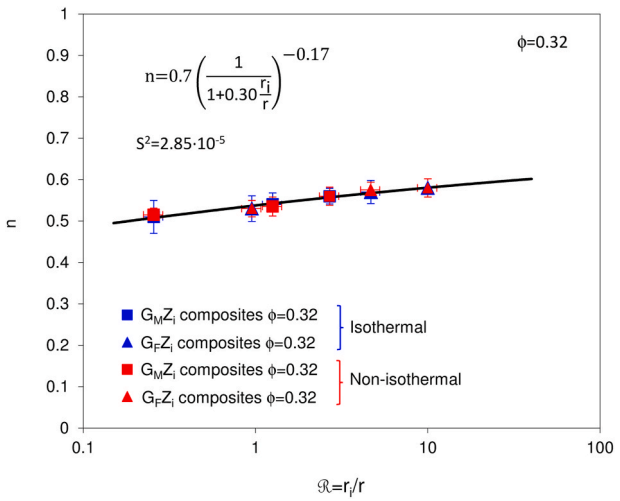

Fig. 16. Effect of size ratio, $\Re = r_i/r$, on the stretching parameter, n. Isothermal (blue symbols) and non-isothermal experiments (red symbols). Composites with ϕ = 0.32. The solid line is the fit to the equation shown. (For interpretation of the references to colour in this figure legend, the reader is referred to the Web version of this article.)

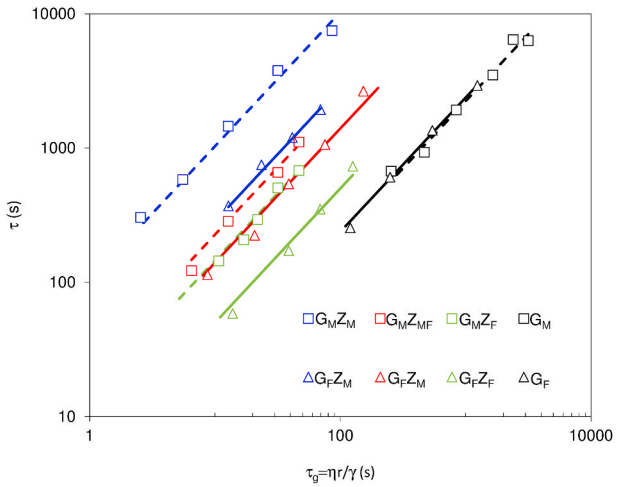

Fig. 17. Relationship between the values of experimental relaxation time, τ, and those of viscous sintering time, τ_g. Glass G_M and G_F (ϕ = 0) and composites with ϕ = 0.32.

Fig. 21.

3.2.3. *Estimation of the rigid percolation threshold, ϕ_p, from the kinetic parameters. Variation of ϕ_p with ϕ and ℜ*

The relation between τ_0/τ_{g0} and τ/τ_g and the zircon volume fraction, ϕ, obtained for composites G_MZ_M (Fig. 6) was also assumed to be valid for other composites, with a different value of ℜ, but having a value of ϕ_p differing from 0.56. That is:

$$\frac{\tau_0}{\tau_{g0}} = \frac{\tau}{\tau_g} = 2\left(1 - \frac{\phi}{\phi_p}\right)^{-4.5} \qquad \text{Eq. 18}$$

Thus, substituting ϕ = 0.32 and the values of τ_0/τ_{g0} and τ/τ_g obtained for each value of ℜ in Eq. (18) the pairs of values (ϕ_p, ℜ) were calculated (Fig. 22). The results exhibited the trend assumed in Fig. 1.

It was verified that ϕ_p increased with the logarithm of ℜ, and for ℜ = 1 (Fig. 22) the value obtained, ϕ_p = 0.61, was very similar to that calculated by simulation for same-sized spheres with frictional contacts between inclusions, ϕ = 0.57 [5].

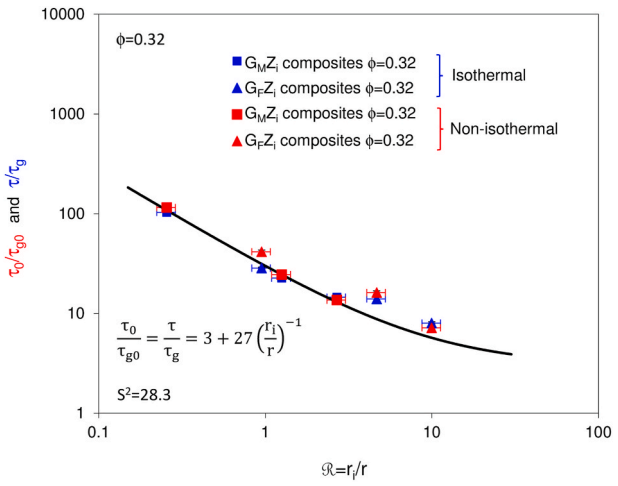

Fig. 18. Effect of ℜ on the values of the ratio τ/τ_g, obtained in isothermal experiments (blue squares), and the ratio τ_0/τ_{g0}, obtained in non-isothermal experiments (red triangles). Composites with $\phi = 0.32$. The solid line is the fit to the equation shown. (For interpretation of the references to colour in this figure legend, the reader is referred to the Web version of this article.)

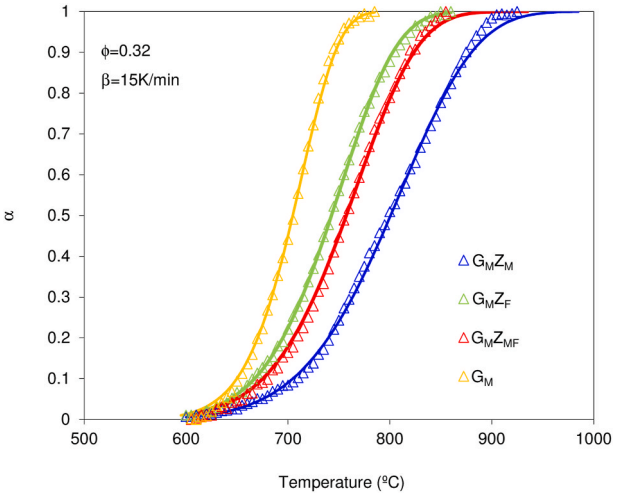

Fig. 19. Effect of zircon size on the non-isothermal sintering curves at $\beta = 15$K/min. The symbols are experimental data, and the solid lines correspond to the values calculated from the model (Eq. (15)). Composites $\phi = 0.32$ prepared with glass G_M, and glass G_M.

3.2.4. Combined effect of ℜ = r_i/r and ϕ on the kinetic parameters of the model: n, τ, or τ_0

For all composites, using the values of ϕ_p calculated from Eq. (18), the values of the ratio ϕ/ϕ_p were determined, this ratio being equivalent to the mass ratio: kg zircon in the composite/kg zircon required for zircon particles to percolate. For all composites, the resulting values of n, both in the isothermal and in the non-isothermal experiments, are plotted versus their respective dimensionless zircon mass ratios, ϕ/ϕ_p, in Fig. 23. Although scattered, the results fitted a straight line of decreasing slope, indicating a linear decrease in the stretching parameter, n, with dimensionless zircon content, ϕ/ϕ_p. Therefore, as the dimensionless zircon content, ϕ/ϕ_p, rose, the number and size of zircon clusters increased, which led to a greater amplitude of the relaxation time distribution, $\rho(\tau_i)$, and hence to an increased sintering range.

The dimensionless values of the ratio: composite relaxation time/glass relaxation time, $\tau/\tau(\phi = 0)$, obtained from isothermal experiments, are plotted versus the respective values of the dimensionless zircon content, ϕ/ϕ_p, for every composite, in Fig. 24. In this figure, the values of the ratio: pre-exponential factor of composite relaxation time/pre-exponential factor of glass relaxation time, $\tau_0/\tau_0(\phi = 0)$, obtained in non-isothermal experiments, are also plotted. All the data fitted very well to a single curve, as had been assumed for $\tau/\tau(\phi = 0)$ (Eq. (7)) and for $\tau_0/\tau_0(\phi = 0)$ (Eq. (12)). In both cases, for $\phi = \phi_p$ the model predicted a composite infinite relaxation time, $\tau = \infty$, and a composite effective viscosity that was also infinite, $\eta_{eff} = \infty$, (Eq. (4)). That is, when a rigid cluster of inclusions formed, for ϕ/ϕ_p, viscous flow densification stopped, $\tau = \infty$, because composite effective viscosity was very high, $\eta_{eff} = \infty$. Analogously, as dimensionless zircon content, ϕ/ϕ_p, increased, the number of zircon particle clusters and their size grew, which in turn raised dimensionless composite relaxation time, $\tau/\tau(\phi = 0)$, and composite relative viscosity, η_{eff}/η.

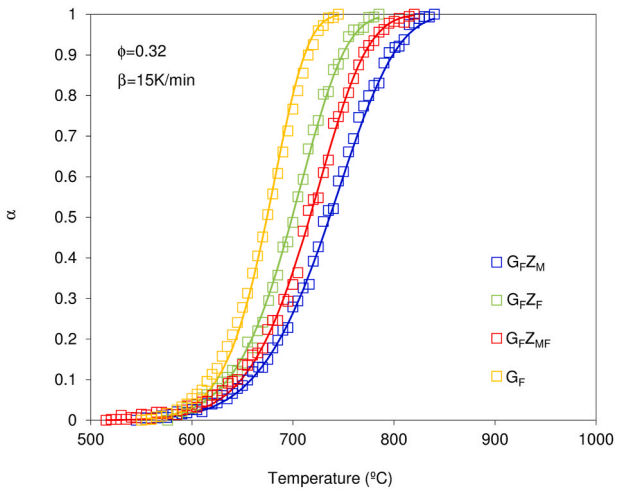

Fig. 20. Effect of zircon size on the non-isothermal sintering curves at $\beta = 15$K/min. The symbols are experimental data, and the solid lines correspond to the values calculated from the model (Eq. (15)). Composites $\phi = 0.32$ prepared with glass G_F, and glass G_F.

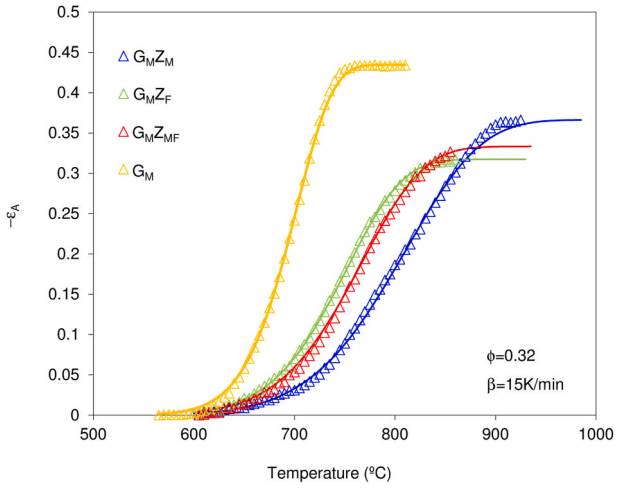

Fig. 21. Effect of zircon size on the curves: surface strain–temperature, ε_A-T, at $\beta = 15$K/min. The symbols are experimental data, and the solid lines correspond to the values calculated from the model (Eq. (15)). Composite $\phi = 0.32$ prepared with glass G_M, and glass G_M.

4. Conclusions

A study was carried out, by isothermal and constant-rate heating experiments, of viscous flow sintering of glass–zircon composites with different zircon contents and different glass and zircon particle size

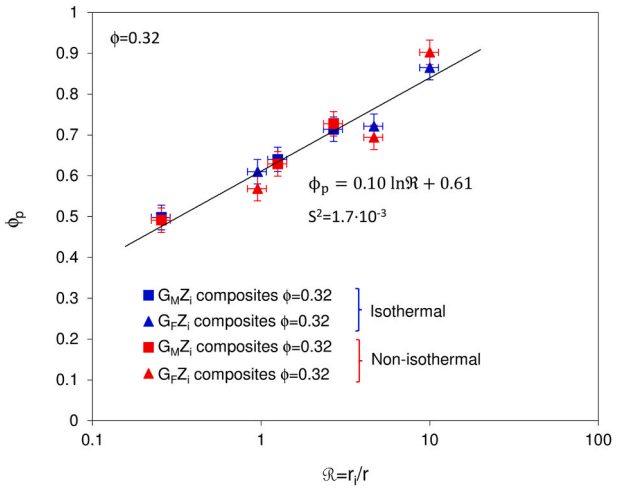

Fig. 22. Variation of the rigid percolation threshold, ϕ_p, calculated from Eq. (18) with ratio $\Re$. Isothermal experiments (blue symbols) and non-isothermal experiments (red symbols). Composites with $\phi = 0.32$. The solid line is the fit to the equation shown. (For interpretation of the references to colour in this figure legend, the reader is referred to the Web version of this article.)

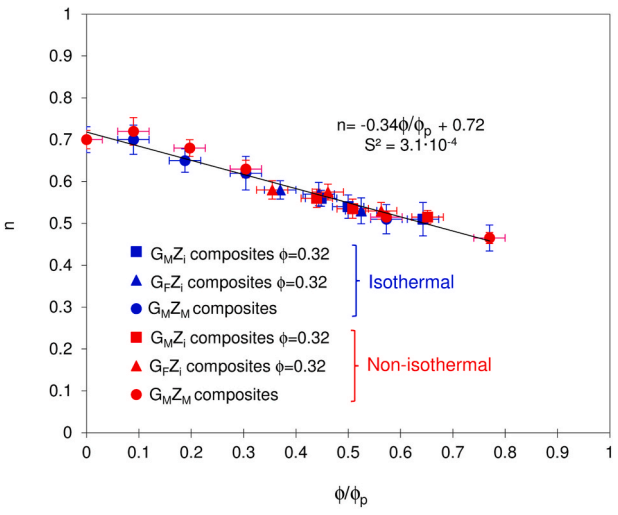

Fig. 23. Variation of stretching parameter, n, with the dimensionless zircon mass ratio, ϕ/ϕ_p. Isothermal (blue symbols) and non-isothermal experiments (red symbols), for all the composites. The solid line is the fit to the equation shown. (For interpretation of the references to colour in this figure legend, the reader is referred to the Web version of this article.)

distributions, continuously determining the variations of compact dimensions using a hot stage microscope (HSM).

The sintering curves of the resulting glass and composite compacts in isothermal and constant-rate heating experiments fitted very well to the developed kinetic model, based on the Kohlrausch–Williams–Watts (KWW) function, in which the stretching parameter, n, depended on the zircon volume fraction, ϕ, and zircon–glass particle size ratio, $\Re$, and the relaxation time constant, τ, depended on these variables and on temperature.

The influence of temperature on process kinetics was verified to correspond to that of this variable on relaxation time, τ, which was proportional to glassy phase viscosity, η. The relationship of τ and η to temperature was accurately described by the Vogel–Fulcher–Tammann (VFT) equation.

Increasing the zircon volume fraction from $\phi = 0$ to $\phi = 0.43$, keeping the ratio between mean zircon and glass particle size constant,

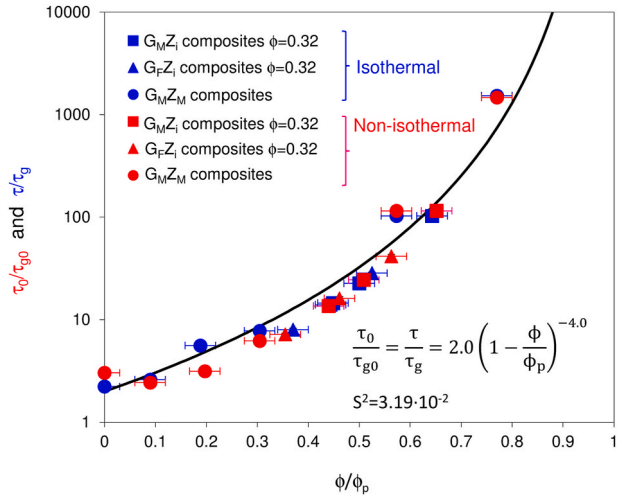

Fig. 24. Effect of dimensionless zircon mass ratio, ϕ/ϕ_p, on the values of the ratio $\tau/\tau(\phi = 0)$, obtained in isothermal experiments (blue symbols), and the ratio $\tau_0/\tau_0(\phi = 0)$, obtained in non-isothermal experiments (red symbols), for all the composites. The solid line is the fit to the equation shown. (For interpretation of the references to colour in this figure legend, the reader is referred to the Web version of this article.)

$\Re = 0.26$, slowed down the sintering rate. The effect of ϕ on the sintering curves in isothermal and constant-rate heating was accurately described by the increase in relaxation time, τ, and decrease in the stretching parameter, n. These relationships were independent of the thermal treatment used.

As the size ratio increased from $\Re = 0.26$ to $\Re = 10$, keeping the zircon volume fraction, $\phi = 0.32$, constant, the sintering rate rose. The effect of $\Re$ on the sintering curves in isothermal and constant-rate heating was accurately described by the decrease in relaxation time, τ, and the increase in the stretching parameter, n. These relationships were also independent of the thermal treatment used.

The combined effect of ϕ and $\Re$ on process kinetics was appropriately described by determining the influence of the ratio between the zircon volume fraction and the rigid percolation threshold, ϕ/ϕ_p, on the kinetic parameters of the model. In accordance with percolation theory, ϕ_p increased with the logarithm of $\Re$.

It was verified that, for all the studied glass and composite compacts, the stretching parameter, n, decreased linearly as ϕ/ϕ_p increased, this relationship being independent of the thermal treatment (isothermal and constant-rate heating) used.

In addition, for every studied compact, the ratio between the composite and matrix glass relaxation time, $\tau/\tau(\phi = 0)$, and the ratio between the pre-exponential factor of composite relaxation time and that of the matrix glass, $\tau_0/\tau_0(\phi = 0)$, increased as ϕ/ϕ_p rose, this function being of the same type as that predicted by percolation theory, and it was independent of the thermal treatment (isothermal and constant-rate heating) used.

Declaration of competing interest

The authors declare that they have no known competing financial interests or personal relationships that could have appeared to influence the work reported in this paper.

Acknowledgements

This study was co-funded by the Valencia Region Government through the Valencian Institute for Business Competitiveness (IVACE).

References

[1] A. Jagota, E.D. Boyes, R.K. Bordia, R. Sintering of glass powder packings with metal inclusions, Mater. Res. Soc. Symp. Proc. 249 (1991) 475–480.

[2] G.W. Scherer, Viscous sintering of particle-filled composites, Am. Ceram. Soc. Bull. 70 (6) (1991) 1059–1063.

[3] G.W. Scherer, A. Jagota, Effect of inclusions on viscous sintering, in: Ceramic Transactions, Adv. Compos. Mater. Am. Ceram. Soc 19, 1991, pp. 99–109. Westerville, OH.

[4] F.F. Lange, L. Atteraas, F. Zok, J.R. Porter, Deformation consolidation of metal powders containing steel inclusions, Acta Metall. Mater. 39 (2) (1991) 209–219.

[5] A. Jagota, G.W. Scherer, Viscosities and sintering rates of composite packings of spheres, J. Am. Ceram. Soc. 78 (3) (1995) 521–528.

[6] J.L. Amorós, A. Moreno, E. Blasco, Viscous flow sintering in glass matrix composites with rigid inclusions, Ceram. Mod. Technol. 3 (2019) 155–162.

[7] J.L. Amorós, E. Blasco, A. Moreno, E. Zumaquero, C. Feliu, Non-isothermal sintering of powdered vitrified composites. A kinetic model, Mater. Lett. 236 (2019) 236–239, https://doi.org/10.1016/j.matlet.2018.10.089.

[8] R. Müller, M. Eberstein, S. Reinsch, W.A. Schiller, J. Deubener, A. Thiel, Effect of rigid inclusions on sintering of low temperature co-fired ceramics, Phys. Chem. Glasses B 48 (4) (2007) 259–266.

[9] A. Winkel, R. Meszaros, S. Reinsel, R. Müller, N. Travitzky, T. Fei, P. Greil, L. Wondraczev, Sintering of 3D printed glass/HAp composites, J. Am. Ceram. Soc. 11 (95) (2012) 3387–3393.

[10] E. Blasco, Sinterización de compactos de vidrio y composites vidrio-circón. Mecanismo y cinética del proceso, Castellón (Spain): PhD Dissertation, Universitat Jaume I. Department of Chemical Engineering, 2017.

[11] J.L. Amorós, E. Blasco, C. Feliu, A. Moreno, Densification of irregular polydispersed glass particles described as a complex relaxation process, Open Ceram 9 (2021) 100205, https://doi.org/10.1016/j.oceram.2021.100205.

[12] J. Amorós, E. Blasco, A. Moreno, M.P. Gómez-Tena, C. Feliu, Non-isothermal sinter-crystallisation of satin glazes: a kinetic model, Ceram. Int. 44 (2018) 7780–7787.

[13] J.L. Amorós, E. Blasco, A. Moreno, N. Marín, C. Feliu, Sinter-crystallisation kinetics of a SiO2-Al2O3-CaO-MgO-SrO glass-ceramic glaze, J. Non-Cryst. Solids 532 (2020) 119900, https://doi.org/10.1016/j.jnoncrysol.2020.119900.

[14] J.L. Amorós, E. Blasco, A. Moreno, N. Marín, C. Feliu, Effect of particle size distribution on the sinter-crystallisation kinetics of a SiO_2-Al_2O_3-CaO-MgO-SrO glass-ceramic glaze, J. Non-Cryst. Solids 542 (2020) 120148, https://doi.org/10.1016/j.jnoncrysol.2020.120148.

[15] M.J. Orts, J.L. Amorós, A. Escardino, A. Gozalbo, C. Feliu, Kinetic model for the isothermal sintering of low porosity floor tiles, Appl. Clay Sci. 8 (1993) 231–245.

[16] S.L. Shamblin, B.C. Hancock, Y. Dupuis, M.J. Pikal, Interpretation of relaxation time constants for amorphous pharmaceutical systems, J. Pharm. Sci. 89 (3) (2000) 417–427.

[17] N. Rabiei, S.H. Amirshahi, M.H. Kish, Description of physical aging kinetics of glassy polymers by interpretation of parameters of the Kohlrausch–Williams–Watts relaxation function via simulation, Am. Phys. Rev. E 99 (3) (2019), 032502.

[18] A. Jagota, G.W. Scherer, Viscosities and sintering rates of a two-dimensional granular composite, J. Am. Ceram. Soc. 76 (12) (1993) 3123–3135.

[19] G. Lois, J. Blawzdziewicz, C.S. O'Hern, Jamming transition and new percolation universality classes in particulate systems with attraction, Phys. Rev. Lett. 100 (2) (2008), 028001.

[20] D. Bouvard, F.F. Lange, Relation between percolation and particle coordination in binary powder mixtures, Acta Metall. Mater. 12 (39) (1991) 3083–3090.

[21] L. Meng, P. Lu, S. Li, Packing properties of binary mixtures in disordered spheres systems, Particuology 16 (2014) 155–166.

[22] D. Chen, Z. Lin, H. Zhu, R.J. Kee, Percolation theory to predict effective properties of solid oxide fuel-cell composite electrodes, J. Powder Sources 191 (2009) 240–252.

[23] C.H. Kuo, P.K. Gupta, Rigidity and conductivity percolation thresholds in particulate composites, Acta Metall. Mater. 43 (1) (1995) 397–403.

[24] M. Suzuki, T. Oshima, Estimation of the co-ordination number in a multi-component mixture of spheres, Powder Technol. 35 (2) (1983) 159–166.

[25] L. Oger, J.P. Troadec, D. Bideau, J.A. Dodds, M.J. Powell, Properties of disordered sphere packings II. Electrical properties of mixtures of conducting and insulating spheres of different sizes, Powder Technol. 46 (2–3) (1986) 133–140.

[26] J.P. Fitzpatrick, R.B. Malt, F. Spaepen, Percolation theory and the conductivity of random close packed mixtures of hard spheres, Phys. Lett. A 47 (3) (1974) 207–208.

[27] M.J. Powell, Site percolation in randomly packed spheres, Phys. Rev. B 20 (10) (1979) 4194–4198.

[28] J.H. Wu, Q. Jia, The heterogeneous energy landscape expression of KWW relaxation, Sci. Rep. 6 (2016) 20506.

[29] P. Murray, J. White, Kinetics of the thermal dehydration of clays. Part IV. Interpretation of the differential thermal analysis of the clay minerals, Trans. Br. Ceram. Soc. 54 (1995) 204–264.

[30] A.P.N. Oliveira, F.G. Rosa, O.E. Alarcon, Effect of the volumetric fraction and particle size on the abrasive mechanism in ceramic glazes, in: QUALICER 94, 1994, Castellón – Spain. Proceedings of the III World Congress on Ceramic Tile Quality II, 1994, pp. 163–175.

[31] A.P.N. Oliveira, O.E. Alarcon, F.G. Rosa, Effect of the volumetric fraction and particle size on the abrasive wear mechanism in ceramic glazes, Int. Ceram. J. (1995) 11–17.

[32] F.M. Bertan, O.R.K. Montedo, C.R. Rambo, D. Hotza, A.P.N. Oliveira, Extruded ZrSiO4 particulate-reinforced LZSA glass-ceramics matrix composite, J. Mater. Process. Technol. 209 (2009) 1134–1142, https://doi.org/10.1016/j.jmatprotec.2008.03.018.

[33] M. Eberstein, S. Reinsch, R. Müller, J. Deubener, W.A. Schiller, Sintering of glass matrix composites with small rigid inclusions, J. Eur. Ceram. Soc. 29 (2009) 2469–2479.

[34] J.L. Amorós, E. Blasco, A. Moreno, C. Feliu, Mechanical properties obtained by nanoindentation of sintered zircon-glass matrix composites, Ceram. Int. 46 (2020) 10691–10695, https://doi.org/10.1016/j.ceramint.2020.01.075.

[35] National Institute of Standards and Technology. Certificate Standard Reference Material 717a Borosilicate Glass.

[36] J.M. Fernández-Navarro, El Vidrio, CSIC, Madrid, 1991.